

GreenScan: Towards large-scale monitoring the health of urban trees using mobile sensing

Akshit Gupta, Simone Mora, Fan Zhang, Martine Rutten, R. Venkatesha Prasad, Carlo Ratti

Abstract—Healthy urban greenery is a fundamental asset to mitigate climate change phenomena such as extreme heat and air pollution. However, urban trees are often affected by abiotic and biotic stressors that hamper their functionality, and whenever not timely managed, even their survival. While current visual or instrumented inspection techniques can help take effective measures, they often require a high amount of human labor, making frequent assessments infeasible at a city-wide scale. In this paper, we present GreenScan, a ground-based sensing system designed to provide health assessment of urban trees at high spatio-temporal resolutions, with low costs. The system utilises thermal and multi-spectral imaging sensors fused using custom computer vision models in order to estimate two tree health indexes. The evaluation of the system was performed through data collection experiments in Cambridge, USA. Overall, this approach illustrates the potential of autonomous mobile ground-based tree health monitoring on city-wide scales at high temporal resolutions with low-costs.

I. INTRODUCTION

URBAN greenery improves cities' resilience to climate change. Nowadays, protecting, managing, and restoring ecosystems is fundamental for climate-resilient development, given the multiple risks posed to humanity and nature by global warming and climate change as per the latest UN-IPCC Report [1]. In urban cities, the tree canopies and vegetation provide a wide range of ecosystem services such as air filtering, carbon sequestration, reduced energy consumption, and decreased local temperatures [2], [3]. However, urban trees are experiencing an ample amount of *abiotic* and *biotic* stressors that are exacerbated due to climate change [4]–[6]. As a result, their functionality, productivity, and survival are of increasing concern [7]. Trees with poor health cannot provide most of their beneficial ecosystem services [8], [9]. For instance, trees with low transpiration rates do not cool the environment sufficiently and trees with low growth rates have a reduced shading effect. By 2050, it is expected that about

This work was supported by the MIT Senseable City Lab Consortium. A. Gupta would like to thank Renswoude Foundation, FAST Delft and EFL Stichting for their financial support.

A. Gupta, M. Rutten and R. V. Prasad are associated with TU Delft (email: a.gupta-5@tudelft.nl, m.m.rutten@tudelft.nl, r.r.venkateshprasad@tudelft.nl)

Akshit Gupta is the corresponding author. He was a visiting student researcher at the MIT Senseable City Lab at the time of this work, while studying at TU Delft.

S. Mora and C. Ratti are with the Senseable City Lab, Department of Urban Studies and Planning, Massachusetts Institute of Technology. (email: moras@mit.edu, ratti@mit.edu)

F. Zhang is with the Department of Civil and Environmental Engineering, The Hong Kong University of Science and Technology. (email: cefzhang@ust.hk)

two-thirds of urban tree species worldwide will fail to provide the desired climate-positive benefits [10].

Nowadays, the health of trees can be inspected by arborists with good quality results, but at high costs due to the amount of human labor involved [11]. Therefore, leading to an assessment that has a low spatial and temporal resolution. In recent years, a few technology-assisted methods have been developed to complement manual inspections. Satellite-based imaging can cover large areas although at a low spatial granularity [12], with data quality depending on the availability of clear skies [12] and low-temporal resolution because satellites revisit the same spot only every few days. Airborne sensing using Unmanned Aerial Vehicles (UAVs) or airplanes leads to an increased spatial granularity [12]; yet it involves high operational costs and may not be suitable in highly urbanized environments due to aviation authority regulations. Further, both airborne sensing and satellite imagery can only capture the overhead view of the urban canopy. As a result, vegetation elements such as green walls, short trees, or shrubs present under the tree canopy may be missed [13] or misinterpreted [14]. These challenges make it economically infeasible for governments and municipalities to perform frequent inspections of urban greenery at a large-scale. As a result, adverse health conditions are often discovered only after severe damage and, sometimes, beyond the point of no return. Further, given the lack of tree health data, intricate relationships of urban trees with other micro-scale ecosystem services is not well understood from an urban planning perspective. For instance, inappropriate placement of trees in outdoor environments can be detrimental as they can serve to reduce and trap air pollutants while also hindering anthropogenic heat [15].

Recently, a number of projects have investigated the use of low-cost technological alternatives to monitor the environmental parameters in cities. For instance, applying Artificial Intelligence (AI) based methods on Google Street View (GSV) images to detect the presence of trees [16], [17], or using drive-by sensing strategies to measure air pollution and other urban morphology parameters [18]. In the case of drive-by sensing (retrofitting vehicles with sensors), it was demonstrated that just ten random taxis could capture data over one-third of streets in Manhattan (New York City) in a single day [19]. Drive-by sensing approaches enable collecting data at both higher temporal and spatial resolutions compared to manual inspection approaches, embedded sensors, or satellite-based sensing. Supplementary, citizen science-based approaches [20] have also been successful in measuring urban environmental parameters such as air pollution [21]. All these methods are set within the domain of opportunistic sensing and are aimed

Approach		Working Mechanism	Quality of Assessment	Cost*
Manual inspection		Depends on method	Generally high, varying based on method	\$\$\$\$
Embedded sensing		Depends on method	High but lower than manual inspection	\$\$\$
Handheld imaging	Hyper/multi-spectral imaging	Properties of chlorophyll (photosynthesis) and cell structure	High-quality quantitative value	\$\$
	Thermal imaging	Cavities, temperature gradient and water stress	Cavities: qualitative value, water stress and temperature gradient: quantitative value	\$
	LiDAR	Geometrical parameters such as Leaf Area Index (LAI) and leaf density	Low-quality quantitative value	\$ to \$\$
Street-view based (visible spectrum)		Uses image processing to quantify amount of greenery	No health assessment, only quantity of greenery	\$
Remote sensing (hyper/multi-spectral, thermal imaging, LiDAR)		Depends on the type of imaging	Top-level view only	\$

TABLE I: A comparison of sensing approaches along with suitable deployment strategies to analyse tree health
(* refers to relative cost where \$ is the lowest cost and \$\$\$ is the highest cost for large-scale evaluation of multiple trees)

at developing platforms that can be deployed and operated without the need of an expensive or a dedicated infrastructure.

Following on this trend and the critical need for protecting and managing urban ecosystems, in this work, we investigate how to measure the health of urban trees, terrestrially, at high spatial and temporal resolutions with low costs for wide-accessibility. The system described in this paper namely, *GreenScan*, measures the health of urban trees on a city-wide scale using complementary indexes that represents a tree's photosynthetic capacity and a tree's water stress levels. The system fuses data from low-cost thermal and multispectral imaging sensors using custom computer vision models to generate two popular health indexes namely NDVI (Normalised Difference Vegetation Index) and CTD (Canopy Temperature Depression). NDVI is based on the optical properties of chlorophyll and cell structure in the leaves [22], while CTD is physically related to the overall water stress of the trees [23]. A *GreenScan* system is suitable for deployment in a citizen-science paradigm by being carried by pedestrians and in a drive-by sensing paradigm by mounting on urban vehicles such as taxis and garbage trucks. Thus, allowing large-scale monitoring the health of trees at high spatial and temporal resolutions for cities and municipalities around the world.

In this paper, we first give a brief overview of the existing state-of-the-art technology supported tools and methods to monitor health of urban greenery and identify the relevant research gaps. We use this to motivate the design of our system and define the architecture of *GreenScan*. A concrete implementation of both the hardware and software components is also described. We evaluate the performance of the system in measuring the health of trees while also discussing the performance of the efficiency optimised computer vision model. We conclude by identifying the immediate future work enabled through large scale deployment of *GreenScan* and illustrate the overall potential of autonomous ground-based tree health monitoring.

II. RELATED WORK

A comparison of the surveyed methods currently used for tree health monitoring in terms of working mechanism, cost, and quality of assessment is shown in Table I.

Manual inspection involves the work of arborists (a tree doctor) inspecting each tree visually, often with the aid of tools

like borers (to extract a wooden core sample from the tree for laboratory analysis) or resistographs (to measure the electrical resistance of the trunk). These methods usually provide high-quality assessment, but they are time-consuming due to the amount of human labor involved to perform a tree-by-tree assessment. Further, although effective, methods that require drilling and penetration in the living wood may create an entry path for pathogens or may alter the structural integrity of a tree. For a review on these methods, see [11].

Embedded sensing involves the deployment of either physical or chemical sensors, which are attached on or near the tree of interest. The physical property under scrutiny can vary, from the detection of sudden vibrations to the measurement of water uptake and transpiration. Usually, this family of methods generates data at high temporal resolutions with little or no human supervision required; yet at the cost of installing and maintaining one or more sensors per tree. For a review on these methods, see [24].

Imaging-based methods involve the use of optical sensors such as thermal imaging sensors, multispectral or hyperspectral imaging sensors or LiDAR (Light Detection and Ranging). Thermal imaging is based on IR (InfraRed) radiation emitted from biological materials and it is mainly used to (i) measure cavities in the living wood, (ii) detect infections caused by insects and bacteria, and (iii) calculate water stress levels by measuring the temperature of the leaves in the canopy. On the other hand, multi/hyper-spectral imaging captures various bands in the electromagnetic spectrum, usually near-infrared and parts of visible spectrum. This captured data is utilised to calculate various vegetation indexes, the most popular being Normalized Difference Vegetation Index (NDVI) which requires the visible red radiation and the Near InfraRed (NIR) radiation reflected by the vegetation. High NDVI values are a proxy for good health or healthy photosynthetic capacity. Low NDVI values are a proxy for overall poor health, the presence of stress or parasites, or the absence of vegetation elements [25]. Light Detection and Ranging (LiDAR) sensors, can be utilised to measure geometrical parameters such as the leaves surrounding a branch, trunk diameter, etc. and to estimate the Leaf Area Index (LAI) [26]. These imaging based approaches are non-invasive since they don't require any physical contact with the tree, in comparison to embedded sensing and manual inspection approaches.

Recently, street-view based methods based on visible RGB

(Red, Green, Blue) images such as [27]–[30], involving the use of google-street view images are emerging. While these approaches are cost-effective and scalable, they are only able to quantify the extent of urban greenery at a terrestrial level rather than its health.

Finally, remote sensing utilising imaging-based sensors deployed on satellites, and Unmanned Aerial Vehicles (UAVs) or airplanes enable high spatial coverage. However, satellites have a low temporal resolution due to infrequent re-visit time over the same spot and the data quality is dependent on the availability of clear skies [12]. Data collection using UAVs and airplanes involves high operational costs and is unsuitable for highly urbanised environments due to aviation regulations. Most importantly, both airborne sensing and satellite imagery can only capture an overhead view of urban tree canopies. As a result, lower vegetation elements such as green walls, short trees, or shrubs are often missed or misinterpreted [13]. For a review on these methods, see [31].

A. Research gaps and influence on design

Comparing different approaches, it emerges that manual inspection methods are infeasible to be deployed on city-side scales due to the high costs and the amount of human labour involved. Further, a subset of these methods involve the use of invasive tools. While deploying imaging-based sensors on satellites and drones can cover large areas; the resulting images have pixels with low spatial granularity, low temporal resolutions due to revisit time [12], and only provide an overhead view of the vegetation. Further, the presence of background materials such as grass or shrubs and clouds in the atmosphere affects the reliability of observations [32].

In contrast, ground-based sensing approaches combined with imaging-based sensors can look at vegetation elements in a holistic manner. For instance, utilising thermal cameras to analyze health attributes such as water stress index and cavities appears theoretically suitable and promising. Hyperspectral/multispectral imaging can also generate a number of vegetation health indexes, the most popular of which is NDVI. Contradictory studies were observed on the usage of LiDAR with some works such as [33] claiming no increase in health classification performance with its addition. Overall, except for a few works utilising imaging-based methods for terrestrial monitoring such as [34], [35], the remaining surveyed works required the use of manual handheld sensor data collection along with manual data processing. Thus, incorporating substantial human labor due to the absence of automated processes, thereby constraining the attainable spatial and temporal resolutions. With the advancements in computer vision and deep learning, in GreenScan, we utilise both multi-spectral and thermal imaging sensors to autonomously measure tree health indexes from ground-level.

B. Comparison with comparable earlier works

Our work is unique in the sense that it is suitable to be deployed for large-scale monitoring of trees without any human intervention. Earlier works in the field which measured tree health terrestrially and used low cost sensors are shown

concisely in Table II along with the research gaps in them and how our work fills this research gap. The two utmost comparable works; [35] requires manual human analysis of images and [12] outputs only raw values without ground truth validation combined with controlled upward facing deployment respectively. Our work fulfills this research gap by being completely autonomous and suitable to be deployed for opportunistic sensing along with validated ground truth data provided by a municipality.

Works	Autonomous (No human intervention needed)	Approach	Ground Truth Comparison	Evaluation
[12]	Yes	Mobile (Cars)	No	172 trees (only system output as no compa- rison)
[36] and [37]	Yes	Handheld	Yes	44 images (trees not mentioned)
[34]	Yes	Handheld	No	8 trees
[38] and [39]	Yes	Mobile (Robot)	Yes	2 trees in controlled lab envi- ronment
[35]	No	Mobile (Cars)	Yes	20 trees
Our work	Yes	Mobile (Cars) and Citizen Science	Yes	40 trees

TABLE II: A concise comparison of our work with comparable earlier works in the field.

III. METHODOLOGY

A. System Architecture

The block diagram of the entire GreenScan system architecture is shown in Figure 1. Herewith, we give a brief description of all the other major modules, as shown in the architecture diagram. The first five modules are related to hardware, while the remaining four modules are related to software.

All the hardware components were encased in a 3D printed case as shown in Figure 2. The case was designed such that it is suitable to be attachable to moving vehicles without any alterations using magnets, as shown in Figure 3.

1) *Hardware Modules*: Below, we first provide the generic description of each hardware module followed by the concrete implementation of the same in our prototype GreenScan system.

1. Thermal Imaging Sensor: A thermal imaging sensor with radiometric calibration (to measure true temperature) is attached to the central single board computer and captures long-wave infrared images normalised to a suitable temperature range with low pixel resolution. A narrow temperature range is preferred to decrease the effect of non-linear noise across the sensor and the low cost thermal imaging sensors are constrained in terms of resolution. This long-wave infrared imaging data is used for generation of CTD (Canopy

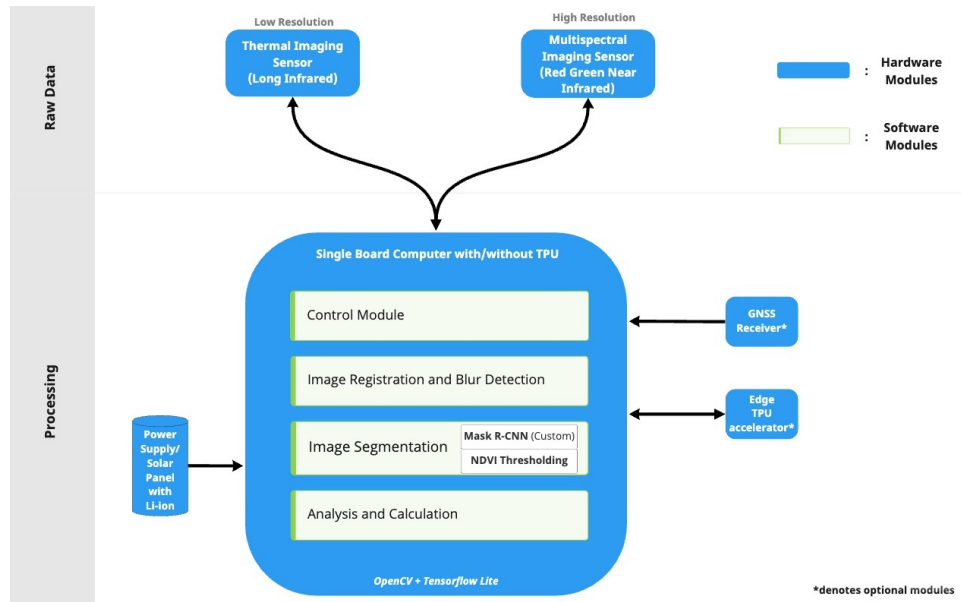


Fig. 1: Architecture Diagram of the GreenScan system

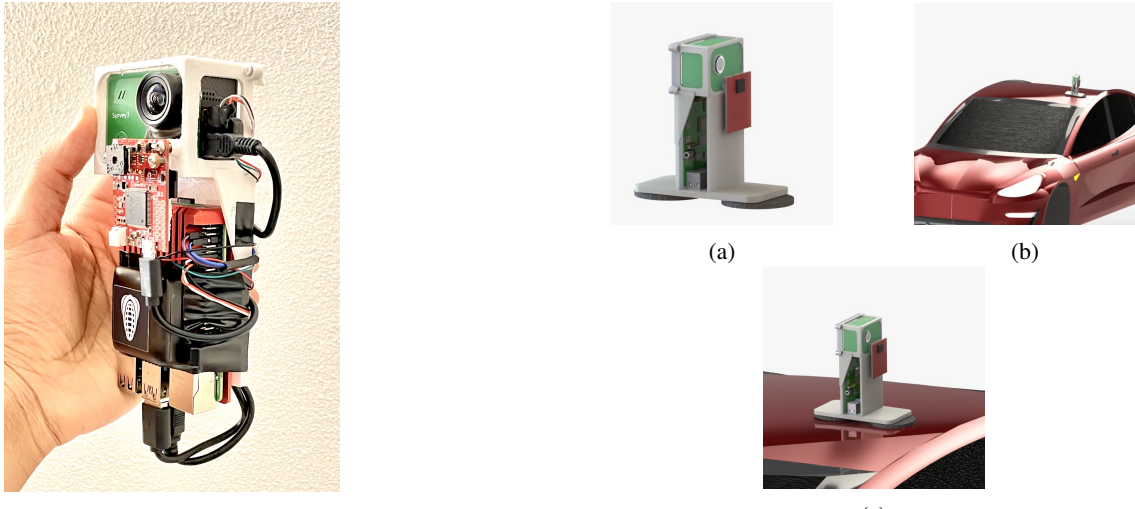


Fig. 2: All hardware components encased with the 3D printed case

Temperature Depression). In future, this thermal imaging data can also be used for detection of cavities in the trunk of the trees as proposed in [40]. However, this was skipped in our prototype mainly due to the low-resolution of the thermal imaging sensor.

For concrete implementation, we used FLIR Lepton 3.5 (spectrum: longwave-infrared @8 μm - 14 μm) attached to an OpenMV cam H7 using a FLIR Lepton adapter module. This captured thermal images with a pixel resolution of 160×120 which are normalised to a suitable temperature range (-10° to 40° C). This temperature range was chosen based on the lowest and highest temperature ($\pm 10^\circ$ C) of trees found during the data collection experiments (in Section IV). The OpenMV cam H7 communicates with Raspberry Pi via remote procedure call (RPC) over USB.

2. Multispectral imaging sensor: A multispectral imaging

Fig. 3: Concept casing: (a) Concept casing for the system with magnets; (b) The system attached to the top of a car; (c) A closeup view of the system attached to the roof of a car

sensor is attached to the central single board computer and captures Red, Green and Near-infrared (RGN) imaging data with high pixel resolution. The near-infrared and red imaging data is used for generation of the NDVI (Normalised Difference Vegetation Index). Further, this high resolution imaging data is used for segmentation of the tree canopy from the images using the custom deep learning model as described in the *Image Segmentation Module*.

For implementation, MAPIR Survey 3W (spectrum: red@660nm, green@550nm, near-infrared@850nm) was attached to the Raspberry Pi over USB and captured RGN imaging data with a pixel resolution of 4000×3000 . To control the MAPIR Survey 3W for triggering the capture and

transfer of images, pulse width modulation (PWM) signals over the micro-HDMI port of MAPIR Survey 3W are used.

3. GNSS Receiver: A Global Navigation Satellite System (GNSS) receiver with support for GPS, GLONASS, and Galileo is used to find the current location of the system and geo-tag all the images of the trees captured.

For our prototype, the RGN images captured were geo-tagged using the standard GPS adapter available for MAPIR Survey 3W.

4. Single Board Computer with/without Edge TPU: A single board computer without/with onboard edge Tensor Processing Unit (TPU) co-processor/USB edge TPU accelerator (such as USB TPU accelerator from coral.ai) acts as the central brain of the system integrating all the hardware and software components. The edge TPU allows to speed up deep learning operations, improving the images processed per second without sending any data to the cloud.

Raspberry Pi 3 was utilised as the single board computer in the GreenScan system running the software modules (see Section III-A2).

5. Power Supply / Solar Panel: A lithium-ion battery (10000 mAh) is used to ensure uninterrupted power supply to the system along with support for charging over a solar panel or a standard power adapter (5V/2A).

2) *Software Modules:* Herewith, we provide the description of each software module followed by the concrete implementation of the same in the GreenScan system. A visualization of processing the images after each software module is also shown in Figure 4.

1. Control Module: This module handles all the embedded communication with the hardware. It includes detecting the event trigger, signaling the sensors to capture the images, and transferring the captured images to the central single board computer.

The event trigger signals the beginning of processing on the Raspberry Pi and in the current prototype, a press of a push button is used as an event trigger for the data collection experiments. This event trigger can also be the co-location of the system with particular GPS coordinates fetched from a tree inventory database. For the thermal imaging sensor, this involves the initiation of callbacks requesting the transfer of the current image frame from FLIR Lepton 3.5. For the multispectral imaging sensor, this involves generating PWM signals to capture an image, mounting the memory card installed in the MAPIR Survey 3W with the Raspberry Pi, transferring the captured image to Raspberry Pi, and finally, unmounting the memory card from the Raspberry Pi.

2. Image Registration: Image registration involves matching or aligning images taken by two different sensors into a single coordinate system for further analysis [41]. It includes detecting key points from one image and mapping them to another image. Since both the multispectral and thermal imaging sensors have different FOVs (field of view) and are un-aligned, this module aligns the multispectral images to the thermal images through linear translation in both horizontal and vertical directions. Also, to compensate for wider FOV of the multispectral sensor, this module also handles zooming in

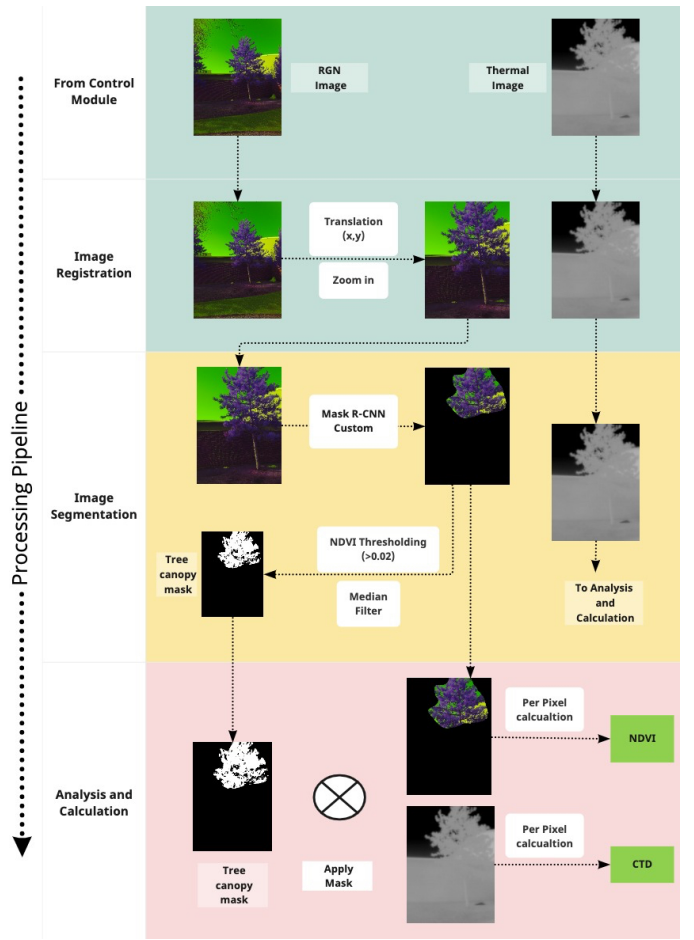


Fig. 4: A visualisation of processing the images at each software module on the Raspberry Pi

on the multispectral images.

For the current prototype, the values of translation in X and Y directions were found to be +50 (right) and +150 (upwards) pixels respectively and the zoom scale was found to be 0.57 (where 1 indicates no magnification and 0 indicates 100 % magnification) to perfectly overlay the thermal and RGN images. These parameters were found by manually taking multiple RGN and thermal images and overlaying them. An instance of inputs and outputs utilizing this module are shown in Figure 4.

Further, automatic image registration using three image registration algorithms namely SIFT, SURF, and ORB [42] was also tested. However, these algorithms were not able to detect useful keypoints or features in the thermal images possibly due to the low resolution (160x120).

3. Image Segmentation: This is the most computationally intensive software module of the system. Recall that the aim of our system is to calculate the NDVI and CTD values for each tree in the images. However, these values should be calculated only for the leaves in tree canopy excluding the wooden parts, such as the trunk and branches. This is solved using a fusion of custom developed Mask R-CNN and pixel-wise NDVI analysis. Given a multispectral RGN image captured using the multispectral imaging sensor, this task can

be broken into two sub-problems as follows:

- **Detect the canopy part of the trees even in cases where the image contains multiple trees:** This is solved using a custom-developed Mask R-CNN model. The Mask R-CNN model is trained using transfer learning and discussed in more detail in Section III-B. It segments the instances of the tree canopies in the RGN image by generating a mask (segmentation) over them as shown in Figure 6.
- **Remove Noise:** Once the canopy of the tree is detected, the segmentation of only the leaves of the tree without the wooden branches and sky. The non-vegetation elements such as trunks, branches, and sky have very low NDVI values compared to vegetation elements which have significantly higher NDVI. Thus, we employ a thresholding based method which first calculates the individual NDVI of each pixel in the segmentation mask generated by Mask R-CNN and then eliminates pixels with NDVI values below a certain threshold. The calculation of NDVI for each pixel is computed by plugging the raw values of the red and near-infrared channels of the pixel in (4). In order to eliminate noise along the edges of tree canopy, median filtering is also employed.

The end result employing the above two-stage approach gives segmentation of only leaves present in the tree canopy while eliminating the sky, wooden branches, trunk and other street objects such as buildings and cars in the multispectral image. Since both the thermal and multispectral images are registered, the same mask of leaves in tree canopy can also be used for thermal images.

With the MAPIR Survey 3W employed in the prototype, a value of 0.02 was used as the cutoff to eliminate non-vegetation elements in the image. This value was derived using the analysis of the images captured during data collection experiments. An instance of inputs and outputs utilizing this module is also shown in Figure 4.

4. Analysis and Calculation Module: This module handles the calculation of final NDVI and CTD for each tree in the field of view of the imaging sensors.

The CTD value is computed by calculating the raw temperature value for each pixel by converting its color intensity value in the grayscale thermal image as per (2), computing the mean temperature over all pixels in the canopy and subtracting the ambient air temperature from the mean canopy temperature as per (3). CTD is calculated as:

$$CTD = T_{canopy} - T_{air} \quad (1)$$

where T_{canopy} and T_{air} are canopy temperature and air temperature respectively in $^{\circ}$ C.

The temperature of each pixel is calculated as:

$$T_{pixel} = \frac{P_{value}}{255} * (T_{max} - T_{min}) + T_{min} \quad (2)$$

where P_{value} is the pixel value in normalised thermal image, T_{min} and T_{max} are configured temperature range for the thermal imaging sensor respectively (-10° C and 40° C in our case). Then, as per (1), CTD is calculated as:

$$CTD = \overline{T_{pixel}} - T_{air} \quad (3)$$

where $\overline{T_{pixel}}$ is the average canopy temperature for all segmented pixels in the image and T_{air} is the air temperature respectively.

To calculate the NDVI, each pixel in the RGN image is split into its three constituting channels (red, green and near-infrared). The raw NDVI value for each pixel is calculated from red and near-infrared channels as per (4). To compensate for the aperture adjustment, the focal adjustment and other mechanical adjustments performed by the multispectral imaging sensor, the raw NDVI is normalised by applying a correction factor similar to the dynamic range of a camera [43] as shown in (5). NDVI is calculated as:

$$NDVI = \frac{NIR - Red}{NIR + Red}, \quad (4)$$

where NIR and Red are values of near-infrared channel and visible red channel for each pixel respectively. Our corrected NDVI is calculated as:

$$NDVI_{corrected} = \frac{NDVI_{raw}}{|NDVI_{max}|} * |NDVI_{min}| \quad (5)$$

where $NDVI_{raw}$ is the raw NDVI of a pixel, $NDVI_{max}$ and $NDVI_{min}$ are maximum and minimum NDVI values for all pixels in the segmented image.

Finally, the NDVI for the entire canopy is computed by taking the mean over the corrected NDVI values for all pixels consisting of leaves in the segmented tree canopy.

B. Development of Custom Mask R-CNN

For the system to operate autonomously, the images will be captured in an unsupervised fashion. Thus, in addition to multiple trees in a single image, they may contain other objects such as cars, buildings, grass, and snow. Hence, it is imperative to individually identify all the tree canopies in an image and feed them to the calculation and analysis module. The custom mask R-CNN part of the image segmentation module solves this by providing instance segmentation of the tree canopies in the image. To our knowledge, there is no pre-existing model available for instance segmentation of tree canopies or even trees in standard RGB images. The problem is further complicated as our input is RGN (Red, Green, Near-infrared) images from the multispectral imaging sensor instead of standard RGB images. For instance, we found that pre-trained models like Deeplabv3 [44], which can perform semantic segmentation of trees and vegetation on standard RGB images, perform poorly on RGN images.

1) Training Data: Any deep learning model requires training data in order to optimise the weights and activations of the layers. However, there does not exist a dataset with labels for instances of trees or tree canopies for RGN Images. Hence, we manually created the dataset using the RGN images collected during the data collection experiments (See Section IV-B). Each tree canopy in the image was manually annotated using a popular image annotation tool called LabelMe [45]. During annotation, only tree canopies that were completely present in the image were labelled. After this process, our dataset consisted of 51 annotated RGN images with two classes namely tree canopies and background.

2) *Training Process and Training Curve*: Our dataset consists of a relatively small number of images to train a deep learning model like Mask R-CNN from scratch. Transfer learning combined with data augmentation was employed in order to develop a custom model by using an existing model pre-trained on a different dataset. For this, we used a Mask R-CNN pre-trained [46] on COCO [47] (a dataset with 330K images) with ResNet101 as the backbone. We re-trained only the head layers (the top layers without the backbone) on our dataset. The batch size was configured as 4 and the number of epochs was 10. The training was performed on the Google Cloud Platform with a N1 instance with 13GB memory and 2vCPUs. We also generated synthetic data by augmenting the original dataset with flips in the horizontal and vertical directions and applying Gaussian blur. This increased the training dataset size by 50% and acted as a regularizer. The manually annotated dataset (refer Section III-B1) consisting of 51 images was split in the ratio of 70: 30 for training: testing. During re-training, each epoch took approximately 3 hours on the N1 instance. The training curve of the model is shown in Figure 5. It is seen from the training curve that only a small number of epochs are sufficient to reach the optimal validation loss on the test set owing to the retraining of only the head layers. The visual output results from our model are shown in Figure 6.

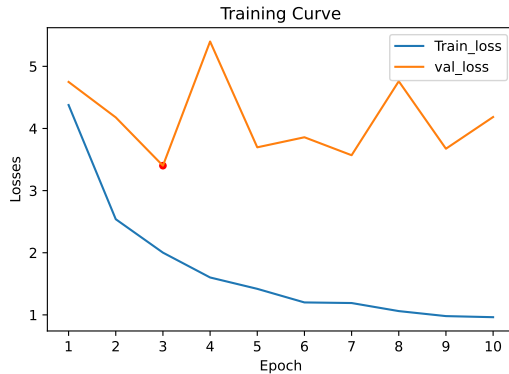
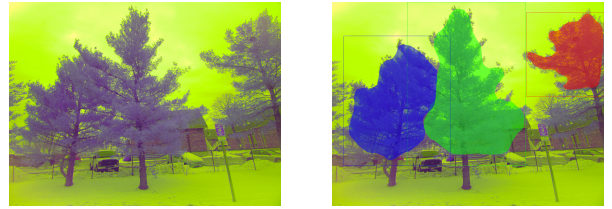


Fig. 5: The training curve of Mask R-CNN with epochs=10 and batch size=4, the red point indicates point of minimum loss, training losses as defined in [48]

3) *Model Quantization*: Mask R-CNN is a relatively heavy model both from training and inference points of view. Hence, the developed Mask R-CNN was optimized to run on the edge at the cost of possible minute performance reduction. For this, the model built on TensorFlow was converted to TensorFlow-lite with dynamic range quantization [49]. Dynamic range quantization means that only the weights of the layers in 32-bit Floats in the full model are stored as 8-bit INTs while the activations of the layers are quantized during runtime. Our custom-made Mask R-CNN built over TensorFlow took around 15 seconds per inference of an image on a Raspberry Pi 4 while the TensorFlow-lite model reduced the inference time to 7 seconds with one-fourth of the CPU usage as the original TensorFlow model.



(a) Input RGN Image captured from MAPIR Survey 3W

(b) Segmentation output from our Custom Mask R-CNN (instance segmentation model) trained using transfer learning

Fig. 6: Performance of our custom Mask R-CNN. Notice how the model detects each instance of the tree canopy in the image and considers all the other objects as background

IV. EVALUATION

We evaluated our system using a ground truth dataset obtained from the municipality of Cambridge, USA. We also conducted three data collection experiments to measure attributes of urban trees using GreenScan. In this section, we elaborate on these datasets followed by the obtained results.

A. (Ground truth) Tree Health Dataset

Municipalities in cities obtain ground truth tree health data through city-wide surveys over years. For instance, in the city of Cambridge, USA, a survey is performed every 5 years whereas, for the city of Delft, The Netherlands, a survey is performed every 2 years. For the evaluation of our work, we obtained a ground truth tree health dataset for the city of Cambridge, USA through the Cambridge Urban Forest Master Plan [14]. A 2018 dataset was obtained through a combination of manual in-person arborist visits, satellite-based remote sensing and aerial LiDAR [14]. The dataset classifies the health conditions of trees into three categories, namely good, poor, and fair. The dataset contains information about 47,063 trees out of which 35,821 are in good health, 5176 are in fair health and 6066 are in poor health. Hence, most of the trees ($> 75\%$) are rated as having a good health condition. In addition, the dataset contains information about the tree species, common name, the satellite-based NDVI, the latitude and the longitude, location, the shape length and shape area of the canopy, flood tolerance, and drought tolerance. This dataset was provided as Shapefiles (.shp, a data format used by Geographical Information Systems (GIS)) and was loaded to the online platform CARTO [50] (a GIS and spatial analysis tool). The staleness of data in terms of time further necessitates the advancement in this field of tree health monitoring.

B. Data Collection Experiments

We collected multispectral (RGN) and thermal images through the developed system on three separate days in Cambridge, USA during the month of February 2022. A push button was used as the event trigger for the system. Hence, we employed the developed GreenScan system as a citizen science project with the 3D printed casing (pedestrian moving at walking speed in a straight line at a distance of 8m - 20m

from the tree). In total, we collected data for 49 trees spread over two species namely Red Pine and Eastern White Pine trees. The multispectral imaging sensor was configured with a shutter speed of 1/60s and ISO of 50. The thermal imaging sensor was configured to measure temperature in range of (-10, 40) °C. The sites of data collection experiments are shown in Figure 7.

Species Constraints: There are two types of trees namely evergreen and deciduous trees. During winters, deciduous trees lose their leaves, thus hampering NDVI calculation. Hence, our analysis was constrained to evergreen trees due to data collection in the winter. The species namely Red pine and Eastern White Pine were selected because they are evergreen and they are the most widespread and easily accessible evergreen trees found from CARTO in the city of Cambridge.

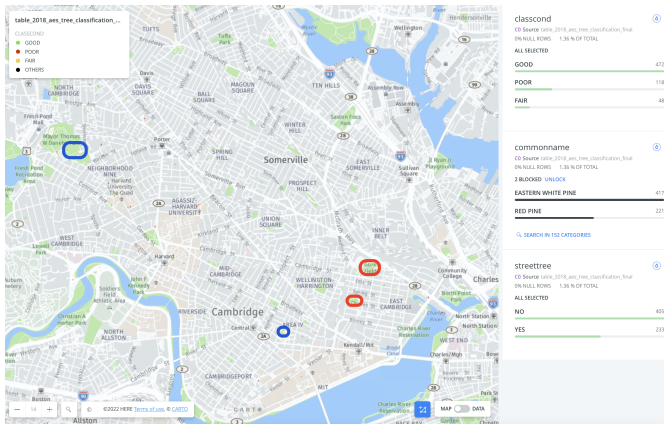


Fig. 7: The trees were analysed in these locations. The red boxes indicate the Red Pine trees and the blue boxes indicate the Eastern White Pine trees.

Data Cleaning: During the first day of the data collection experiments, the Raspberry Pi hung up due to unknown reasons leading to a forced restart. On the third day of the experiments, owing to cold temperatures, the power supply had to be changed during data collection. These interruptions and restarts resulted in unstable values for a sequence of readings related to the canopy temperature by the thermal imaging sensor. As a result, these 11 data points were removed from our dataset generated using data collection experiments. In the end, our dataset was reduced to contain 40 trees. Distribution of the data collected from each of the tree species after data cleaning is shown in Table III.

Species	Number of Trees	Health Distribution
Red Pine	26	Good: 15 Fair: 7 Poor: 4
Eastern White Pine	14	Good: 5 Fair: 1 Poor: 8

TABLE III: Distribution of trees after data cleaning

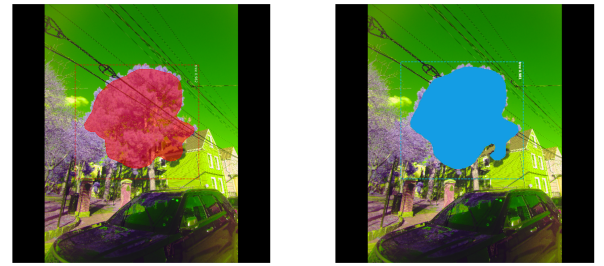
C. Performance of custom Mask R-CNN

To measure the performance of our custom Mask R-CNN model, we calculated the standard evaluation metrics [51] as used by COCO. Specifically, we measured mean Average Precision (mAP) / Average Precision (as per [51]) at different

IoU (Intersection over Union) thresholds. The performance of our custom Mask R-CNN with and without quantization is shown in Table IV. A comparison of inference time and model size comparing both the full model and the quantized model is also shown in Table IV. In order to measure the stability of our results, k-Fold cross-validation was also performed with k=3, to evaluate the performance of the model on different training and test splits as shown in Table V. These results for different train-test splits as shown in Table V showcase the reliability of our model. From Table IV, it is seen that there is no significant reduction in performance using quantization. The inference time of the quantized model is half compared to the non-quantized model along with the reduction of the model size.

An example of segmentation outputs generated by the full model and quantized model on the same image is also shown in Figure 8. This also showcases the similar performance for both the full and the optimised model in a visual form.

From Table , it may appear that the $AP^{(IoU=0.5:0.95:0.05)}$ for the quantized model is increased slightly compared to the full model. On further exploring this anomaly, it was found that this behaviour is exhibited due to our annotated dataset where most images contain only one full tree canopy as ground truth. Thus, a model (non-quantized model) generalising better to find partially visible tree canopies, in addition to the full tree canopy is penalised in terms of Precision (False Positive). Further, it is seen from Figure 9 that the performance of the quantized model decreases more than the full model at higher IoUs (IoU= 0.85 for quantized model compared to 0.90 for full model) signifying that it is slightly poorer at object localisation compared to the full model.



(a) Segmentation output from Mask R-CNN using full Tensorflow model
(b) Segmentation output from Mask R-CNN using Tensorflow-lite (quantized)

Fig. 8: Outputs from custom Mask R-CNNs in Tensorflow and Tensorflow-lite

D. Results for the health of trees

We extracted three parameters from the ground truth dataset namely Ground Truth Condition (Health), Remote NDVI, and Area of the tree (measured using aerial LiDAR) from all the parameters present in the dataset.

A comparison of our system-measured NDVI and Remote NDVI is shown in Figure 10. As seen in this Figure, our measured NDVI is distributed similarly to the Remote NDVI for an individual tree (denoted by Tree Index in Figure 10) .

Model	$AP(IoU=0.5:0.95:0.05)$	$AP(IoU=0.5)$	$AP(IoU=0.75)$	InferenceTime	ModelSize
Custom Mask R-CNN TF	0.489	0.938	0.500	15s	255.9 MB
Custom Mask R-CNN TF-lite (Dynamic Quantization)	0.491	0.938	0.500	7s	65 MB

TABLE IV: Performance of custom R-CNN model (Full and Quantized model)

Cross Validation Fold	1	2	3
$AP(IoU=0.5)$	0.82	0.87	0.75

TABLE V: Results of 3-Fold Cross Validation of custom Mask R-CNN model

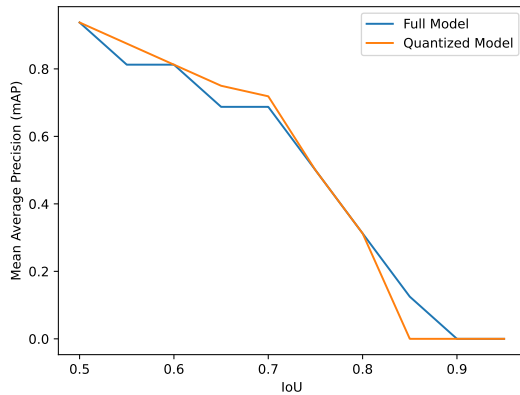


Fig. 9: The AP scores with increasing IoU thresholds as per COCO metrics [47] for the full and quantized tf-lite model

Pearson's correlation coefficient (r) was measured to calculate the strength of the linear relationship between our measured values and ground truth data. The correlation matrix comprising all of our measured values with the three ground truth parameters namely Ground Truth Condition, Remote NDVI, and Area is shown in Figure 11. Further, the correlation results between the measured NDVI and CTD with ground truth parameters is shown in Table VI. From Table VI, it is seen that there is a moderately strong correlation ($r=0.54$ with $p < 0.05$) between our measured NDVI and remote NDVI. For context, in recent works [52], the correlation between NDVI measured using two different satellites was found to be 0.74. Two datasets can be highly correlated but strongly disagree. Hence, a Bland-Altman plot [53] widely used to showcase the agreement between two measurement methods (instead of the strength of relationship as indicated by Pearson's coefficient) is shown in Figure 12. From the Bland-Altman plot, it is seen that there is strong agreement between the two methods (Remote NDVI and Terrestrial NDVI) with 98% (more than 95%) points lying between average difference ± 1.96 standard deviation of the difference limits.

The distribution of CTD and NDVI with respect to ground truth health conditions is shown in Figure 13. From the NDVI distribution in Figure 13a, it is seen that the extent of agreement of NDVI with respect to the ground truth health conditions varies with respect to the species. For red-pine

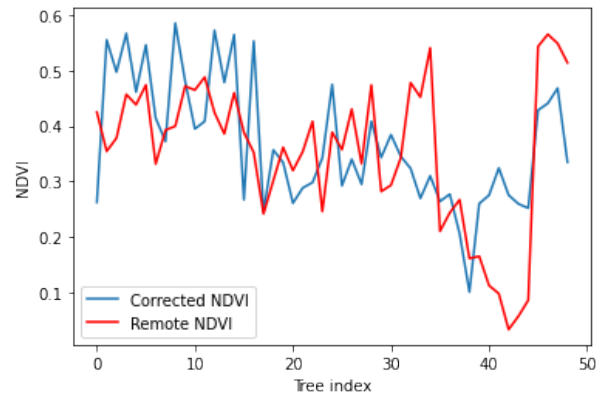


Fig. 10: Variation of measured NDVI vs Remote NDVI for trees observed during data collection experiments

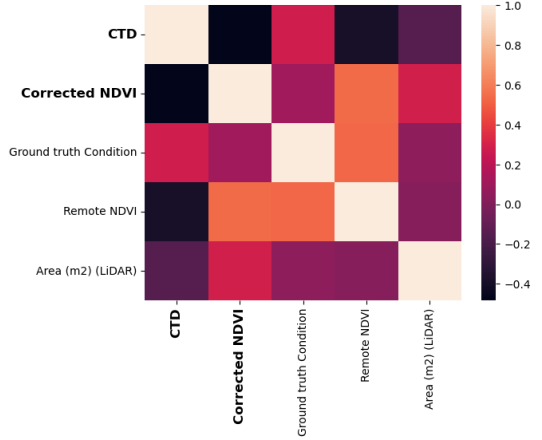


Fig. 11: Correlation matrix between our measured values (in bold) and parameters from ground truth dataset

trees, the trees in good health condition have higher measured NDVI values than trees in poor and fair condition. A similar conclusion is drawn from the CTD distribution in Figure 13b. The mean NDVI and CTD for each species is also shown in Table VII.

1) *High-level tree health analysis*: From Figure 11, it is clear that there is almost no correlation between NDVI and CTD. Thus, they are independently measuring two different attributes related to tree health and useful to incorporate in the system. Further, in recent works such as [52], the correlation between remote NDVI measured using two different satellites was found to be 0.74 (moderately strong). From Table VI, the moderately strong correlation ($r=0.54$ with $p < 0.05$) between our measured NDVI (ground based) and remote NDVI can be mainly due to the time drift (four years apart) between the measurements. In any case, this moderately strong correlation

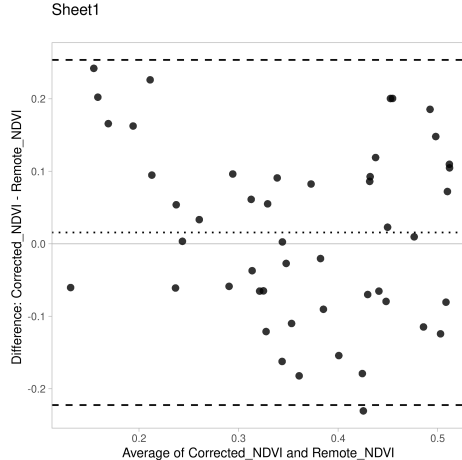


Fig. 12: The Bland-Altman plot showcasing the agreement between Corrected NDVI and Remote NDVI. The dashed-middle line shows the mean difference. The top most and bottom most lines indicate the upper and lower lines of agreement respectively.

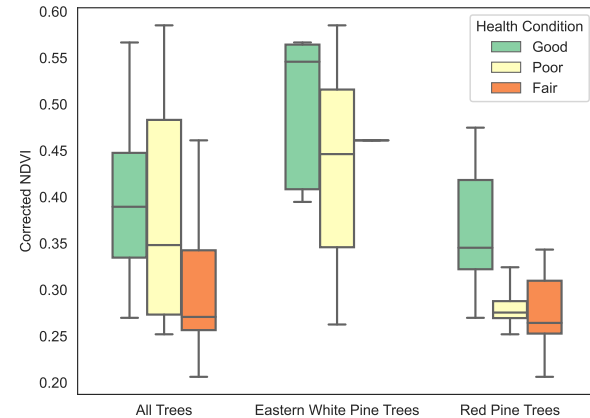
Variables		Pearson Correlation	Significant at
Measured	Ground Truth	(r)	($p < 0.05$)
NDVI	Remote NDVI	0.54	Yes
CTD	Remote NDVI	-0.38	No
NDVI	Health Condition	0.11	No
CTD	Health Condition	0.28	Yes
NDVI	Area (m ²) (LiDAR)	0.28	Yes
CTD	Area (m ²) (LiDAR)	-0.15	No

TABLE VI: The correlation between our measured values and ground truth parameters

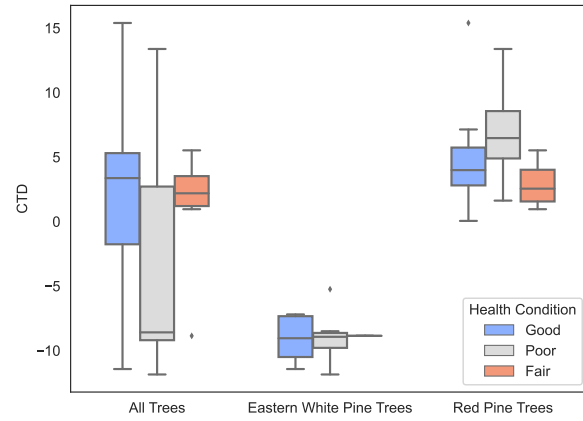
serves to showcase the validity of our approach. The weak-moderate correlation ($r=0.28$ with $p < 0.05$) between CTD and ground truth tree health condition can be attributed to the skewed distribution of the dataset where more trees are rated as having good conditions compared to poor and fair conditions. Further analysis of CTD distribution for all trees in Figure 13b shows the high variability of CTD for trees in poor condition leading to this overall weak-moderate correlation. Interestingly, due to unknown reasons, NDVI is found to have a significant and weak moderate correlation ($r=0.28$ with $p < 0.05$) with the area of tree canopy obtained from the ground truth dataset in Table VI.

2) *Species-wise tree health analysis:* It is inferred from Table VII and Figure 13, that the distribution of NDVI values are in agreement with the health condition of trees for both red pine and eastern white pine species. In fact, mean NDVI values for Red pine as shown in Table VII are significant ($p < 0.05$) for good and poor condition trees. The mean NDVI values for Eastern White Pine trees are insignificant ($p > 0.05$ considering the three different tree health conditions). However, from the NDVI distributions for Eastern White pine in Figure 13a, it is seen that the good condition trees are generally distributed to have higher NDVI values than poor and fair condition trees.

From Figure 13b, while a higher CTD is found for red pine



(a) The distribution of NDVI for the trees



(b) The distribution of CTD for the trees

Fig. 13: The distribution of NDVI and CTD for the trees with respect to health

Species / Health	Good	Fair	Poor
Red Pine (NDVI)	0.37 ± 0.07	0.28 ± 0.05	0.28 ± 0.03
Eastern White Pine (NDVI)	0.49 ± 0.08	0.46	0.43 ± 0.12
Red Pine (CTD)	4.63 ± 3.64	2.89 ± 1.78	6.99 ± 4.85
Eastern White Pine (CTD)	-9.1 ± 1.88	-8.59	-9.1 ± 1.88

TABLE VII: The mean of measured NDVI and CTD across species and health

trees in poor condition than good and fair health condition trees, the same pattern is not applicable for eastern white pine trees. This inference about CTD is similar to earlier works such as [37] [36], where the tree species under observation has a significant influence on the results obtained from thermal imaging. Hence, further studies with varied species are required to measure the stability of CTD with respect to ground truth health conditions.

V. LIMITATIONS AND FUTURE WORK

Subsequent investigations stemming from this work and using our approach as a foundational framework are expected to illuminate and solve several novel challenges, subset of which are delineated as follows.

1) *Feasibility of modelling-based classification:* From the correlation matrix in Figure 11, it is seen that there is no correlation between CTD and NDVI values. Hence, to develop an autonomous model to classify tree health, both these measured parameters are useful. A scatter plot between NDVI and CTD values for red pine trees is shown in Figure 14. From the scatter plot, it is seen that most of the fair and poor-condition trees are concentrated around a cluster between NDVI (0.20-0.35) and CTD (0-7). Hence, simple white-box machine learning algorithms like SVMs with kernel [54] or logistic regression classifiers [55] can be used to autonomously distinguish between good, poor, and fair condition trees. Further, the methodology can be expanded by adding human-in-the-loop-validation at intermediate steps to enhance the performance of the system.

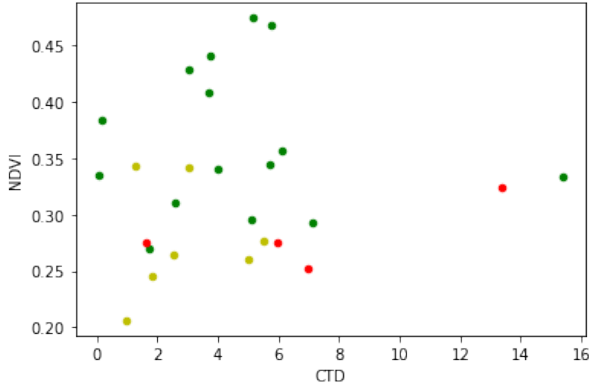


Fig. 14: Scatter plot between NDVI and CTD for red pine trees. The color of the points indicates the ground truth health with red denoting poor, yellow denoting fair, and green denoting good condition trees.

2) *Direction of movement and Robust positioning system:* At present, our methodology is contingent upon aligning the system consisting of the imaging sensors with the trees' orientation. However, given the intended practical application in real-world scenarios, the angle between the tree canopy and the camera's direction could potentially impact the segmentation of tree canopies. Furthermore, our current positioning method relies on GPS coordinates sourced from the tree survey dataset and the GNSS module within the system, which inherently faces uncertainties in positioning. Thus, an alternative positioning approach that integrates GNSS with computer vision techniques may offer enhanced robustness.

3) *Real-time segmentation using Mask R-CNN:* While the results of the k-fold cross-validation as shown in Table V showcase the reliability of our results, the inference time as shown in Table IV is still high for real-time image processing. Since our system does not need to be instantaneous based on the use case, batch processing can be applied after the collection of images at regular intervals in a real-world deployment

scenario. For instance, the system can process the captured data while the moving vehicle is waiting at traffic lights.

4) *Scalability in different weather conditions and geographical boundaries:* The effect of different weather conditions with reduction of visibility, and sunlight directly facing the imaging sensor lenses needs further exploration. Secondly, the deployment and validation of the system in cities with different topographies and with geographical domain shifts can help in enhancing the generalization of the approach using large-scale training and validation datasets.

VI. CONCLUSION

Urban greenery provides various environmental services such as carbon sequestration, and cooling making them essential for building climate-adaptive cities. Currently, urban trees are experiencing atypical amounts of natural and human-induced stresses leading to their volatile health. Yet, high costs make it infeasible for cities to perform frequent inspections on a large scale, leading to adverse health conditions being discovered only after severe damage. The current popular methods for monitoring the health of urban trees rely on an in-person inspection performed by arborists and remote sensing based on satellites or airborne imagery. However, all these methods are riddled with various challenges involving scalability, spatio-temporal resolutions, and quality of assessment. In this work, we developed a novel system to measure tree health autonomously from the ground level in urban cities. The system fuses data from low-cost thermal and multispectral imaging sensors using custom computer vision models optimised for efficiency to generate the tree health indexes namely NDVI and CTD. The custom Mask R-CNN model fine-tuned using transfer learning was employed to fuse the data collected by the imaging sensors on the edge device. Deployment can be performed both in a drive-by sensing paradigm on moving vehicles such as taxis and garbage trucks or in a citizen-science sensing paradigm by humans. Evaluation of the system was performed through data collection experiments in Cambridge, USA. The custom Mask R-CNN developed performed admirably, with an $AP^{IoU=0.50} = 0.938$ despite the small dataset used for training. The tree health analysis revealed moderately-strong correlation ($r=0.54$ with $p-value < 0.05$) between our measured NDVI and the remote NDVI obtained from the ground truth dataset. Further, for both the species of trees analysed, our measured NDVI distributions were found to be in theoretical agreement with ground truth tree health conditions. For CTD, a pattern with a theoretical agreement was applicable for one of the species observed. In essence, this work illustrates the potential of autonomous ground-based tree health monitoring on city-wide scales at high temporal resolutions while motivating future research at the intersection of environmental science and computer science.

REFERENCES

[1] "Climate change 2022: Impacts, adaptation and vulnerability." [Online]. Available: <https://www.ipcc.ch/report/sixth-assessment-report-working-group-ii/>

[2] E. Gregory McPherson, "Accounting for benefits and costs of urban greenspace," *Landscape and Urban Planning*, vol. 22, no. 1, pp. 41–51, 1992. [Online]. Available: <https://www.sciencedirect.com/science/article/pii/016920469290006L>

[3] S. E. Hobbie and N. B. Grimm, "Nature-based approaches to managing climate change impacts in cities," *Philosophical Transactions of the Royal Society B: Biological Sciences*, vol. 375, no. 1794, p. 20190124, jan 2020. [Online]. Available: <https://doi.org/10.1098%2Frstb.2019.0124>

[4] N. Grimm, S. Faeth, N. Golubiewski, C. Redman, J. Wu, X. Bai, and J. Briggs, "Global change and the ecology of cities," *Science (New York, N.Y.)*, vol. 319, pp. 756–60, 03 2008.

[5] S. A. Nitolslawski, N. J. Galle, C. C. K. van den Bosch, and J. W. N. Steenberg, "Smarter ecosystems for smarter cities? a review of trends, technologies, and turning points for smart urban forestry," *Sustainable Cities and Society*, 2019.

[6] IPCC, *Summary for Policymakers*. Cambridge, United Kingdom and New York, NY, USA: Cambridge University Press, 2021, p. 3-32.

[7] Z. R. Werbin, L. Heidari, S. Buckley, P. Brochu, L. J. Butler, C. Connolly, L. Houttuyn Bloemendaal, T. D. McCabe, T. K. Miller, and L. R. Hutyra, "A tree-planting decision support tool for urban heat mitigation," *PLOS ONE*, vol. 15, no. 10, pp. 1–13, 10 2020. [Online]. Available: <https://doi.org/10.1371/journal.pone.0224959>

[8] K. L. Hand and K. J. Doick, "Understanding the role of urban tree management on ecosystem services." [Online]. Available: <https://www.forestreresearch.gov.uk/research/understanding-role-urban-tree-management-ecosystem-services/>

[9] D. R. Hilbert, L. A. Roman, A. K. Koeser, J. Vogt, and N. S. van Doorn, "Urban tree mortality: A literature review," *Arboriculture & Urban Forestry (AUF)*, vol. 45, no. 5, pp. 167–200, 2019. [Online]. Available: <https://auf.isa-arbor.com/content/45/5/167>

[10] K. Huang, "Urban forests facing climate risks," *Nature Climate Change*, vol. 12, no. 10, pp. 893–894, 2022.

[11] E. Leong, D. Burcham, and Y. Fong, "A purposeful classification of tree decay detection tools," *Arboricultural Journal*, vol. 34, 06 2012.

[12] S. Fuentes, E. Tongson, and C. Gonzalez Viejo, "Urban green infrastructure monitoring using remote sensing from integrated visible and thermal infrared cameras mounted on a moving vehicle," *Sensors*, vol. 21, no. 1, 2021. [Online]. Available: <https://www.mdpi.com/1424-8220/21/1/295>

[13] X. Li, C. Zhang, W. Li, R. Ricard, Q. Meng, and W. Zhang, "Assessing street-level urban greenery using google street view and a modified green view index," *Urban Forestry & Urban Greening*, vol. 14, no. 3, pp. 675–685, 2015. [Online]. Available: <https://www.sciencedirect.com/science/article/pii/S1618866715000874>

[14] "Cambridge urban forest master plan preliminary report." [Online]. Available: <https://www.cambridgema.gov/-/media/Files/publicworksdepartment/urbanforestmasterplan/technicale-portappendix.pdf>

[15] N. H. Wong, T. Tan, D. Kolokotsa, and H. Takebayashi, "Greenery as a mitigation and adaptation strategy to urban heat," *Nature Reviews Earth & Environment*, vol. 2, 01 2021.

[16] X. Li, C. Zhang, W. Li, R. M. Ricard, Q. Meng, and W. Zhang, "Assessing street-level urban greenery using google street view and a modified green view index," *Urban Forestry & Urban Greening*, vol. 14, pp. 675–685, 2015.

[17] I. Seiferling, N. Naik, C. Ratti, and R. Proulx, "Green streets: Quantifying and mapping urban trees with street-level imagery and computer vision," *Landscape and Urban Planning*, vol. 165, pp. 93–101, 09 2017.

[18] A. Anjomshoaa, F. Duarte, D. Rennings, T. J. Matarazzo, P. Desouza, and C. Ratti, "City Scanner: Building and Scheduling a Mobile Sensing Platform for Smart City Services," *IEEE Internet of Things Journal*, vol. 5, no. 6, pp. 4567–4579, 2018.

[19] K. P. O'Keeffe, A. Anjomshoaa, S. H. Strogatz, P. Santi, and C. Ratti, "Quantifying the sensing power of vehicle fleets," *Proceedings of the National Academy of Sciences*, vol. 116, no. 26, pp. 12 752–12 757, 2019. [Online]. Available: <https://www.pnas.org/doi/abs/10.1073/pnas.1821667116>

[20] J. Silvertown, "A new dawn for citizen science," *Trends in Ecology & Evolution*, vol. 24, no. 9, pp. 467–471, 2009. [Online]. Available: <https://www.sciencedirect.com/science/article/pii/S016953470900175X>

[21] European Environment Agency, *Assessing air quality through citizen science*. The European Commission, 2020.

[22] C. J. Tucker, "Red and photographic infrared linear combinations for monitoring vegetation," *Remote Sensing of Environment*, vol. 8, no. 2, pp. 127–150, 1979.

[23] M. Balota, W. A. Payne, S. R. Evett, and M. D. Lazar, "Canopy temperature depression sampling to assess grain yield and genotypic differentiation in winter wheat," *Crop Science*, vol. 47, no. 4, pp. 1518–1529, 2007.

[24] C. Torresan, M. Benito Garzón, M. O'Grady, T. M. Robson, G. Picchi, P. Panzacchi, E. Tomelleri, M. Smith, J. Marshall, L. Wingate, R. Tognetti, L. E. Rustad, and D. Kneeshaw, "A new generation of sensors and monitoring tools to support climate-smart forestry practices," *Canadian Journal of Forest Research*, vol. 0, no. 0, pp. 1–15, 0. [Online]. Available: <https://doi.org/10.1139/cjfr-2020-0295>

[25] S. Huang, L. Tang, J. Hupy, Y. Wang, and G. Shao, "A commentary review on the use of normalized difference vegetation index (ndvi) in the era of popular remote sensing," *Journal of Forestry Research*, vol. 32, 05 2020.

[26] J. Degerickx, D. Roberts, J. McFadden, M. Hermy, and B. Somers, "Urban tree health assessment using airborne hyperspectral and lidar imagery," *International Journal of Applied Earth Observation and Geoinformation*, vol. 73, pp. 26–38, 2018.

[27] X. Li, C. Ratti, and I. Seiferling, "Quantifying the shade provision of street trees in urban landscape: A case study in boston, usa, using google street view," *Landscape and Urban Planning*, vol. 169, pp. 81–91, 2018. [Online]. Available: <https://www.sciencedirect.com/science/article/pii/S0169204617301950>

[28] Y. Zhang, S. Li, X. Fu, and R. Dong, "Quantification of urban greenery using hemisphere-view panoramas with a green cover index," *Ecosystem Health and Sustainability*, vol. 7, no. 1, p. 1929502, 2021. [Online]. Available: <https://doi.org/10.1080/20964129.2021.1929502>

[29] N. Y. YIXI XIA and T. FUKUDA, "Development of an urban greenery evaluation system based on deep learning and google street view," 2020. [Online]. Available: http://papers.cumincad.org/data/works/att/caadria2020__028.pdf

[30] C. Wei, Meng, W. Zhiwei, Z. Yong, and Y. Jaemo, "Evaluating greenery around streets using baidu panoramic street view images and the panoramic green view index," *Forests*, vol. 10, p. 1109, 12 2019.

[31] A. Lausch, S. Erasmi, D. J. King, P. Magdon, and M. Heurich, "Understanding forest health with remote sensing -part i—a review of spectral traits, processes and remote-sensing characteristics," *Remote Sensing*, vol. 8, no. 12, 2016. [Online]. Available: <https://www.mdpi.com/2072-4292/8/12/1029>

[32] Y. Wei, H. Wang, K. F. Tsang, Y. Liu, C. K. Wu, H. Zhu, Y.-T. Chow, and F. H. Hung, "Proximity environmental feature based tree health assessment scheme using internet of things and machine learning algorithm," *Sensors*, vol. 19, no. 14, 2019. [Online]. Available: <https://www.mdpi.com/1424-8220/19/14/3115>

[33] S. Rosli, F. Hashim, T. Raj, W. M. D. W Zaki, and A. Hussain, "A rapid technique in evaluating tree health using lidar sensors," *International Journal of Engineering and Technology(UAE)*, vol. 7, pp. 118–122, 08 2018.

[34] C. Kwok, M. Wong, H. Li, K. Hui, F. Ko, H. Shiu, and Z. Kan, "Detection of structural tree defects using thermal infrared imaging," in *40th Asian Conference on Remote Sensing: Progress of Remote Sensing Technology for Smart Future, ACRS 2019*, 2020.

[35] J. Y. Kim and D. M. Glenn, "Multi-modal sensor system for plant water stress assessment," *Computers and Electronics in Agriculture*, vol. 141, pp. 27–34, 2017. [Online]. Available: <https://www.sciencedirect.com/science/article/pii/S0168169916311073>

[36] C. Ballester, M. A. Jiménez-Bello, J. R. Castel, and D. S. Intrigliolo, "Usefulness of thermography for plant water stress detection in citrus and persimmon trees," *Agricultural and Forest Meteorology*, vol. 168, pp. 120–129, 2013.

[37] M. Jiménez-Bello, C. Ballester, J. Castel, and D. Intrigliolo, "Development and validation of an automatic thermal imaging process for assessing plant water status," *Agricultural Water Management*, vol. 98, pp. 1497–1504, 08 2011.

[38] M. Bietresato, G. Carabin, D. D'Auria, R. Gallo, G. Ristorto, F. Mazzetto, R. Vidoni, A. Gasparetto, and L. Scalera, "A tracked mobile robotic lab for monitoring the plants volume and health," in *2016 12th IEEE/ASME International Conference on Mechatronic and Embedded Systems and Applications (MESA)*, 2016, pp. 1–6.

[39] R. Vidoni, R. Gallo, G. Ristorto, G. Carabin, F. Mazzetto, L. Scalera, and A. Gasparetto, "Byelab: An agricultural mobile robot prototype for proximal sensing and precision farming," 11 2017, p. V04at05a057.

[40] A. Catena and G. Catena, "Overview of thermal imaging for tree assessment," *Arboricultural Journal*, vol. 30, 03 2008.

[41] E. Kamoun, "Image registration: From sift to deep learning," Mar 2021. [Online]. Available: <https://www.sicara.ai/blog/2019-07-16-image-registration-deep-learning>

- [42] "Opencv: Feature detection and description." [Online]. Available: https://docs.opencv.org/3.4/db/d27/tutorial_py_table_of_contents_feature2d.html
- [43] "Dynamic range in digital photography." [Online]. Available: <https://www.cambridgeincolour.com/tutorials/dynamic-range.htm>
- [44] L.-C. Chen, G. Papandreou, F. Schroff, and H. Adam, "Rethinking atrous convolution for semantic image segmentation," Dec 2017. [Online]. Available: <https://arxiv.org/abs/1706.05587>
- [45] Wkentaro, "Wkentaro/labelme: Image polygonal annotation with python (polygon, rectangle, circle, line, point and image-level flag annotation)." [Online]. Available: <https://github.com/wkentaro/labelme>
- [46] W. Abdulla, "Mask r-cnn for object detection and instance segmentation on keras and tensorflow," https://github.com/matterport/Mask_RCNN, 2017.
- [47] "Common objects in context." [Online]. Available: <https://cocodataset.org/#home>
- [48] K. He, G. Gkioxari, P. Dollár, and R. Girshick, "Mask r-cnn," Jan 2018. [Online]. Available: <https://arxiv.org/abs/1703.06870>
- [49] "Post-training quantization tensorflow lite." [Online]. Available: https://www.tensorflow.org/lite/performance/post_training_quantization
- [50] Carto, "Location intelligence & gis for cloud natives." [Online]. Available: <https://carto.com/>
- [51] "Common objects in context evaluation metrics." [Online]. Available: <https://cocodataset.org/#detection-eval>
- [52] A. Cogato, V. Pagay, F. Marinello, F. Meggio, P. Grace, M. De, and M. Migliorati, "Assessing the feasibility of using sentinel-2 imagery to quantify the impact of heatwaves on irrigated vineyards," *Remote Sensing*, vol. 11, pp. 1–19, 12 2019.
- [53] J. Martin Bland and D. Altman, "Statistical methods for assessing agreement between two methods of clinical measurement," *The Lancet*, vol. 327, no. 8476, pp. 307–310, 1986, originally published as Volume 1, Issue 8476. [Online]. Available: <https://www.sciencedirect.com/science/article/pii/S0140673686908378>
- [54] J. Cervantes, F. Garcia-Lamont, L. Rodriguez-Mazahua, and A. Lopez, "A comprehensive survey on support vector machine classification: Applications, challenges and trends," *Neurocomputing*, vol. 408, pp. 189–215, 2020. [Online]. Available: <https://www.sciencedirect.com/science/article/pii/S0925231220307153>
- [55] J. Peng, K. Lee, and G. Ingersoll, "An introduction to logistic regression analysis and reporting," *Journal of Educational Research - J EDUC RES*, vol. 96, pp. 3–14, 09 2002.

Simone Mora is a Research Scientist at the Massachusetts Institute of Technology (MIT). He does research on novel sensing technologies and their applications for future sustainable cities. He develops methods and tools for rapid design and rapid prototyping of internet-connected sensors and human-computer interfaces. Dr. Mora holds a PhD degree in Computer Science from NTNU (Norway) and a MSc degree in Computer Engineering from UniBg (Italy). During his graduated studies, he has been a visiting scholar at City London University and MIT. In 2018 he co-founded a company that developed an ideation toolkit to tackle the UN's Sustainable Development Goals. Dr. Mora co-authored more than fifty publications in peer-reviewed international journals. He serves as guest editor for the MDPI Electronics journal and as a reviewer for the Association of Computing Machinery (ACM) and the Institute of Electrical and Electronics Engineers (IEEE).

Fan Zhang received the B.E. degree in electronic engineering from the Beijing Normal University, China in 2012, the M.Sc. and Ph.D. degree in GeoInformation Science from the Chinese University of Hong Kong in 2013 and 2017, respectively. From 2017 to 2022, he worked as a senior research associate at Peking University and Massachusetts Institute of Technology. Starting in 2022, he worked as an assistant professor at the Hong Kong University of Science and Technology. His research sits at the intersection of urban Informatics, data-driven approaches for urban studies, and geographic artificial intelligence. Dr Zhang is currently an associate editor of Transactions in Urban Data, Science, and Technology, and a guest editor of ISPRS Journal of Photogrammetry and Remote Sensing. He has served as a reviewer for over 50 SCI journals in GIS and urban studies and was included in Stanford's list of the world's top 2% scientists in 2022. He received the Geospatial World 50 Rising Stars Award in 2022 and the Global Young Scientist Award in Frontier Science and Technology from WGDC in 2020.

Martine Rutten is an associate professor Water Management and Climate adaptation. She has a background in civil engineering with specializations Hydraulic Engineering (ETHZurich) and Water resources management (TUDelft) and a PhD degree on remote sensing for water resources management. She has a broad integrated perspective that is reflected in her research portfolio which spans a wide set of topics, from nexus modelling, to optimal control to citizen science. She has a strong background in transdisciplinary learning for water resources management and vast experience with learning communities and living labs.

Akshit Gupta (M'22) received the B.E. degree in electronics and communication engineering from the University of Delhi, India in 2017 and the M.Sc. degree in Embedded Systems, the M.Sc. degree in Computer Science from the TU Delft, the Netherlands in 2022. He is currently pursuing the Ph.D. degree at TU Delft, the Netherlands. From 2021 to 2022, he was visiting student researcher at the Senseable City Lab, MIT, USA. His specialization in the domain of optimization and networking aspect of embedded systems and the artificial intelligence domain for computer science enables him to modularise and ideate, based on raw hardware and software from the ground up. His current research interest include internet of things, network science, embedded systems, edge AI and likes to solve problems in domains of hardware-based sensing and applied machine learning. Akshit's awards and honors includes annotation entrepreneurship '22 by TU Delft, DJ100 '21 (the 100 sustainable young frontrunners in the Netherlands), the merit scholarship for academic excellence '14-'17 by University of Delhi and winner of multiple hackathons and tech competitions listed at www.iamakshitgupta.com.

R. Venkatesha Prasad received the Ph.D. degree from the Indian Institute of Science, Bengaluru, India. He is an Associate Professor with the Embedded and Networked Systems Group, Delft University of Technology, Delft, The Netherlands. He has participated in several European and Dutch projects in the area of Internet of Things, 60-GHz communications, personal networks, and cognitive radios. He has around 250 publications in the peer-reviewed international journals and conferences. His research interest is in the area of tactile Internet, Internet of Things, 60-GHz MMW networks, and 5G. Dr. Prasad has served on the editorial board of many IEEE TRANSACTIONS. He has contributed to several standards, including IEEE P1918.1 and P1906.1. He is a Senior Member of ACM.

Carlo Ratti received the joint Graduate degree from the Politecnico di Torino and the École Nationale des Ponts et Chaussées and the M.Phil. and Ph.D. degrees from the University of Cambridge, U.K. He is currently the Founder and the Director of the MIT Senseable City Laboratory. An architect, and an engineer by training, he practices in Italy and teaches at the Massachusetts Institute of Technology. He has co-authored over 200 publications and holds several patents. His work has been exhibited worldwide at venues, such as the Venice Biennale; the Design Museum Barcelona; the Science Museum, London; GAFTA, San Francisco; and The Museum of Modern Art, New York. His Digital Water Pavilion at the 2008 World Expo was hailed by Time Magazine as one of the “Best Inventions of the Year.” He has been included in Esquire Magazine’s “Best and Brightest” list, Blueprint Magazine’s “25 People Who Will Change the World of Design,” and Forbes Magazine’s “Names You Need To Know” in 2011. He was a Presenter at TED 2011. He is serving as a member for the World Economic Forum Global Agenda Council for Urban Management.